



SOI nanophotonic waveguide structures fabricated with deep UV lithography

W. Bogaerts^{a,*}, P. Dumon^a, D. Taillaert^a, V. Wiaux^b, S. Beckx^b, B. Luyssaert^a,
J. Van Campenhout^a, D. Van Thourhout^a, R. Baets^a

^aDepartment of Information Technology (INTEC), Ghent University, IMEC, Sint-Pietersnieuwstraat 41,
9000 Gent, Belgium

^bIMEC vzw., Silicon Process Technology Division Kapeldreef 75, 3001 Leuven, Belgium

Received 12 June 2004; received in revised form 7 July 2004; accepted 7 July 2004

Available online 2 August 2004

Abstract

To reduce the dimensions of photonic integrated circuits, high-contrast wavelength-scale structures are needed. We developed a fabrication process for Silicon-on-insulator nanophotonics, based on standard CMOS processing techniques with deep UV lithography. Measurements using either end-fire incoupling or grating-based fibre couplers show photonic crystal waveguides with moderate propagation losses (7.5 dB/mm) and photonic wires with very low propagation losses (0.24 dB/mm).
© 2004 Published by Elsevier B.V.

PACS: 42.82.E; 42.79; 85.60; 42.82.C; 42.81.Q

Keywords: Nanophotonics; Photonic crystal; Photonic wire

1. Introduction

Integration of photonic functions on-chip promises reduction of costs and increased performance. Moreover, alignment can be guaranteed through lithographic processes, eliminating costly active alignment methods. However, today's photonic components are too large for large-scale integration, as waveguides require large bends to confine the light. To

improve confinement, a higher index contrast is needed, but to keep such waveguides single-mode, the cross section must be sufficiently small. In a semiconductor-air/oxide system ($\Delta n > 2$), waveguides have submicron dimensions and are often called *nanophotonic* waveguides. These small features are hard to fabricate with conventional optical lithography. Moreover, coupling to single-mode fibres becomes very difficult.

There are basically two mechanisms for waveguiding in nanophotonic waveguides. One can use conventional guiding in a high-index core surrounded by a low-index cladding. Such *photonic wires* are typically

* Corresponding author. Tel.: +32 9 2643446;
fax: +32 9 2643593.

E-mail address: wim.bogaerts@intec.ugent.be (W. Bogaerts).

300-500 nm wide. Alternatively, one can use a periodic structure, a photonic crystal, with high refractive index contrast and a period of the order of the wavelength of the light [1]. This strong contrast and periodicity can create a photonic band gap (PBG), forbidding the light to propagate through the crystal. When adding a line defect to a photonic crystal, light can be confined to the defect, creating a waveguide. In principle, bends in photonic crystals can be very abrupt. A photonic crystal slab is a 2-D periodic structure where, in the vertical direction, light is confined by total internal reflection. These structures can be fabricated with high-resolution lithography and dry etching in semiconductor.

At telecommunication wavelengths, both photonic wires and photonic crystals have dimensions of a few hundred nanometers. However, the required accuracy is of the order of 10 nm. For research purposes, nanophotonic components are often fabricated with e-beam lithography. While this technique is very accurate, it is too slow for mass-fabrication. Deep UV lithography at 248 or 193 nm, as used for advanced CMOS, offers both high resolution and throughput, and has proven itself in a production environment.

2. Fabrication with CMOS processes

For our high-contrast photonic structures, we use *Silicon-on-insulator* (SOI). The top Silicon layer is a good waveguide core, because its high refractive index ($n = 3.45$) contrasts very well with the underlying

oxide ($n = 1.45$). For our experiments, we used commercial wafers from SOITEC with a Silicon thickness of 220 nm and an oxide layer of 1 μm .

2.1. Deep UV lithography

We made use of the CMOS research facilities of IMEC, Belgium. For lithography, we used an ASML PAS5500/750 248 nm deep UV stepper. The fabrication process for our nanophotonic circuits is shown in Fig. 1. A 200 mm SOI wafer is spin-coated with Shipley UV3 photoresist, pre-baked, and given a top AR coating. Then the stepper illuminates the photoresist, which is then baked again, and developed. The photoresist is used as an etch mask.

A nanophotonic circuit typically consists of a number of very different structures, which, for accurate alignment, should be printed together in a single lithography step. However, not all structures have the same optimal lithography conditions; especially the lithography exposure dose has a strong effect [2,3]. The optimal dose for photonic crystals and photonic wires can differ significantly. To fabricate both simultaneously, a bias needs to be applied on the mask to either one or the other, preferably the isolated wires. Fig. 2 shows the hole diameter and the line width as a function of the exposure dose (in mJ/cm^2). As an example, the optimal dose for a triangular lattice of 300 nm holes with 500 nm pitch is indicated ($25.6 \text{ mJ}/\text{cm}^2$). At this dose, a 500 nm line is printed 450 nm wide. A 50 nm bias for the lines on the mask would result in a correct line width [3,4]. This bias should be known at the design stage. Therefore, our

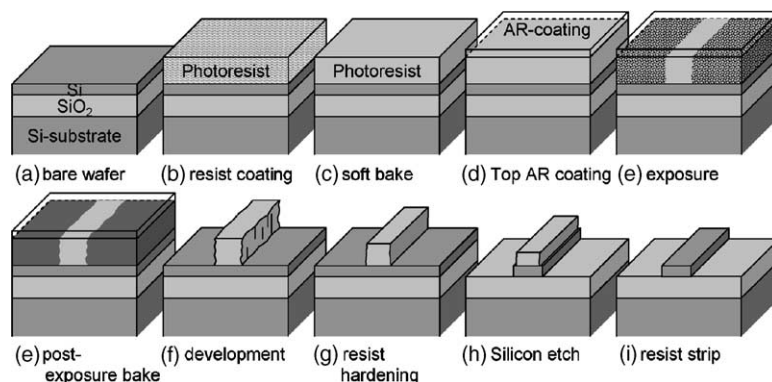


Fig. 1. Fabrication process for photonic nanostructures in SOI using deep UV lithography and dry etching.

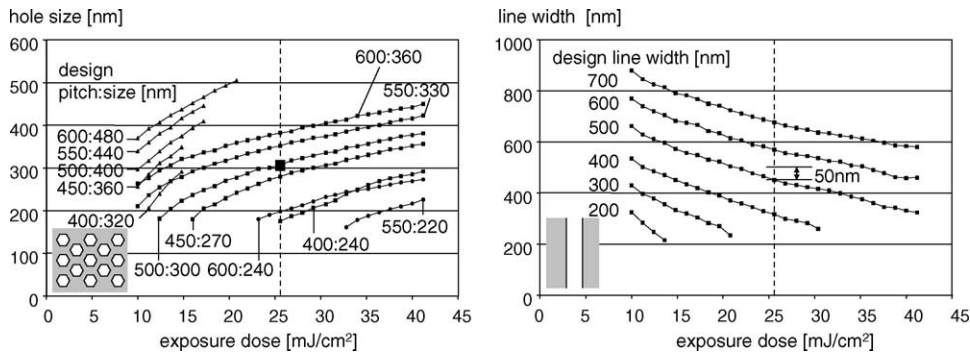


Fig. 2. Hole diameter and line width (in nm) as a function of exposure dose (in mJ/cm^2) for different design parameters.

first mask included many test structures from which we extracted the necessary bias.

2.2. Etching

After lithography, the patterns in the photoresist are etched into the underlying SOI. Before etching the Silicon layer, the photoresist is treated with a plasma, smoothing irregularities in the photoresist patterns. Then, we etched the top Silicon layer using an ICP etch with a $\text{Cl}_2/\text{HBr}/\text{He}/\text{O}_2$ chemistry. Figs. 5a, 6b and 7a show some of the fabricated structures.

3. Measurement setup

To characterise the fabricated structures, we measured the transmission in the wavelength range between 1500 and 1600 nm. However, because of the small dimensions of nanophotonic waveguides,

it is not easy to couple light into the waveguides and collect the transmitted light.

3.1. End-fire measurements

Light from a tunable laser is focused onto the cleaved facet of a $3\ \mu\text{m}$ wide ridge waveguide using a tapered lensed fibre. The wide ridge waveguide is then adiabatically tapered down to a single-mode photonic wire. At the outcoupling side, a taper guides the light back to a $3\ \mu\text{m}$ ridge and a high-NA objective collects the light at the outcoupling facet, projecting it onto a power detector.

3.2. Grating-based fibre couplers

Because Silicon-on-insulator has only a thin core layer, end-fire incoupling is not very efficient, reproducible and stable. Fig. 3a shows a fibre coupler, based on a diffractive grating, to couple from a ridge wave-

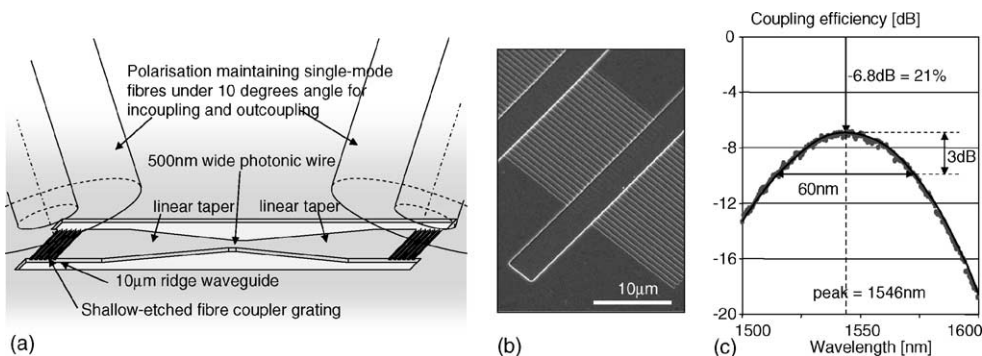


Fig. 3. Measurement with fibre coupling gratings. (a) Measurement setup, (b) SEM picture of a single coupler grating, (c) coupling efficiency of a single fibre coupler.

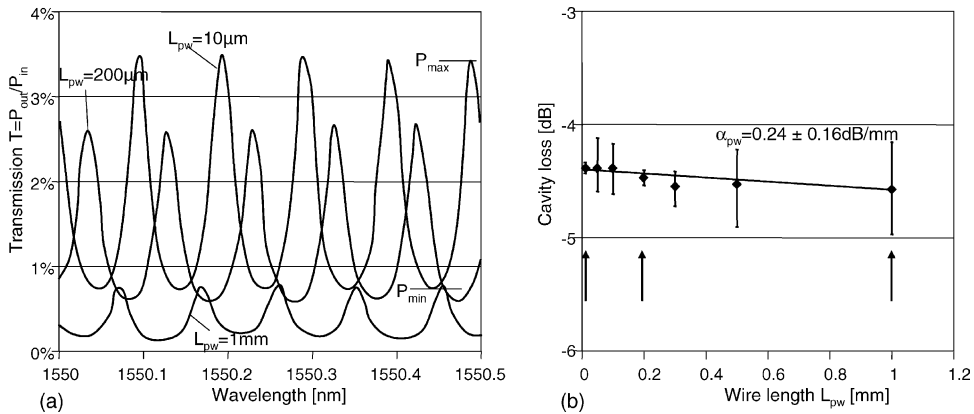


Fig. 4. (a) Transmission spectrum of a Fabry–Perot cavity containing a 500 nm wide photonic wire with a wire length L_{pw} of 10 μm , 200 μm and 1 mm. (b) Cavity loss, expressed in dB, as a function of wire length L_{pw} . The slope of the fit gives the propagation loss in dB/mm. The cavity loss values extracted from the curves in (a) are indicated with arrows.

guide to a vertical butt-coupled single-mode fibre [5]. The grating, shown in Fig. 3b, is etched 50 nm into the Silicon and fabricated in a separate process step [3]. The alignment is guaranteed by the deep UV stepper. The coupling efficiency of such a fibre coupler is shown in Fig. 3c, where -6.8 dB corresponds 21% coupling efficiency, with a 3 dB bandwidth of 60 nm [4].

4. Measurement results

4.1. Photonic wires

We determined the propagation losses of photonic wires by measuring the loss of wires with different lengths. Because these waveguides have very low loss,

we analysed end-fire measurements on a Fabry–Perot cavity formed by cleaved facets. From the periodical transmission characteristic, as shown in Fig. 4a, one can extract the overall cavity loss as a function of the fringe contrast P_{\max}/P_{\min} [6]. The transmission spectrum for 500 nm wide wires with a length of 10, 200, and 1000 μm are shown. Fig. 4b shows the resulting overall cavity loss extracted from each of these measurements as a function of the length of the photonic wire in the cavity. When we now plot these losses (expressed in dB) for cavities containing wires of different length (in mm), as shown in Fig. 4b, we can extract the propagation losses of the wires (in dB/mm) from the slope of the fitted line [7]. We used various wire lengths between 10 μm and 1 mm. This results in a propagation loss of 0.24 dB/mm for

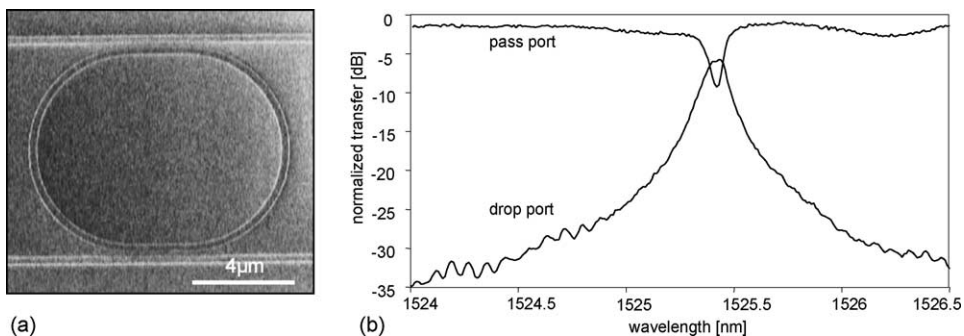


Fig. 5. (a) A racetrack resonator with a bend radius of 4 μm and a straight coupling section of 3.14 μm . (b) Detail of the transmission spectrum of the pass and the drop port of this resonator. The resonator has a Q of over 12,000.

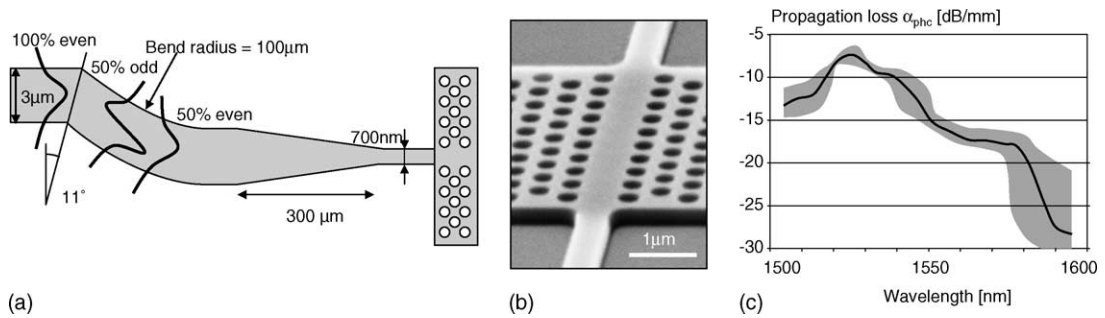


Fig. 6. (a) Mode mixer to excite antisymmetric photonic crystal modes. (b) Micrograph of a W1 photonic crystal waveguide with a pitch of 500 nm and a hole diameter of 320 nm. (c) Propagation losses of the W1 photonic crystal waveguide. The measurement error is indicated by the shaded band.

500 nm wide wires. For narrower wires, losses increase strongly, with 0.74 dB/mm for 450 nm width and 3.4 dB/mm for 400 nm width [4,7]. The wires are multi-mode for widths larger than 550 nm.

We also measured the transmission of ring and racetrack resonators. For the racetrack resonator illustrated in Fig. 5a, we found well defined transmission peaks with a quality factor $Q > 12,000$. A detail of the transmission spectrum of both pass and drop port is shown in Fig. 5b. The resonator has a bend radius of 4 μm and a straight coupling section of 3.14 μm. However, coupling efficiency is less than 40%. We have also demonstrated racetrack resonators with a

lower Q ($Q \approx 3000$), but with a coupling efficiency of over 80%[7].

4.2. Photonic crystal waveguides

Photonic crystal waveguides are more difficult to characterise. Many waveguide designs have a first-order, antisymmetric guided mode. To excite these modes with a symmetric incoupling spot from the lensed fibre or the fibre coupler, we use the mode converter shown in Fig. 6a with an 11° abrupt bend in a 3 μm wide ridge, which splits the even ground mode

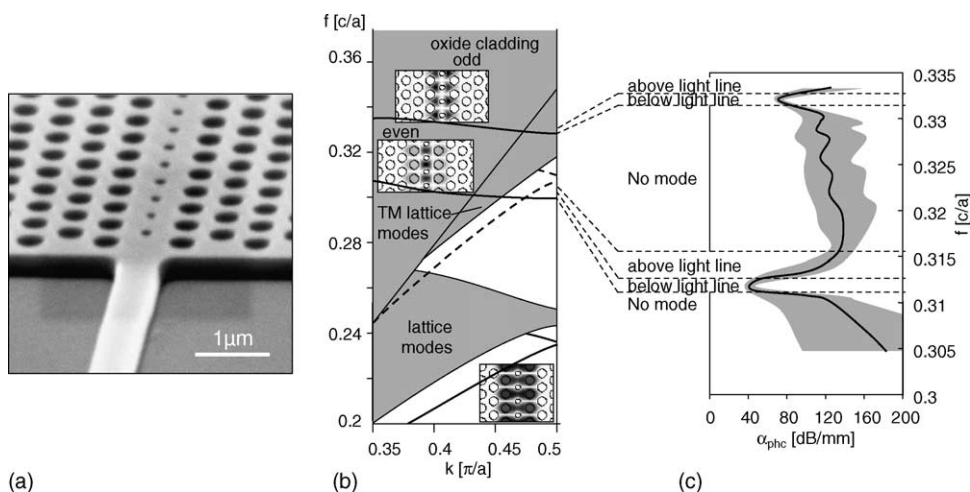


Fig. 7. (a) W1 waveguide with small defect holes. $a = 500$ nm, $\varnothing = 320$ nm in the bulk and the defect hole diameter $\varnothing_{def} = 200$ nm. (b) Detail of the calculated band diagram. (c) Transmission measurement. The measurement error is indicated by the shaded band.

into a 50%/50% combination of the ground mode and the first order mode.

We have fabricated a large number of photonic crystal waveguides with different defect sizes and geometries, using both the straight incoupling waveguides and the 50% mode mixer. Fig. 6c shows the propagation losses of a W1 photonic crystal waveguide with a lattice pitch $a = 500$ nm and holes of 320 nm. Around 1525 nm, the antisymmetric mode is guided and has a propagation loss of 7.5 dB/mm, significantly larger than the losses of the photonic wires. For short waveguides, like the one in Fig. 6, there is still some transmission for the lossy even mode (above the light line), but for longer waveguides, the even mode is filtered out completely. Therefore, when extracting the propagation loss, more weight is given to the longer waveguides.

Fig. 7 shows another photonic crystal waveguide, a W1 with small defect holes with a diameter $\varnothing_{\text{def}} = 200$ nm. Again, the mode mixer is used for incoupling. We can match the regions of low propagation losses exactly to the guided modes in the band diagram. However, the losses are still of the order of 40 dB/mm, due to the large sidewall surface introduced by the defect holes.

5. Conclusions

We used deep UV lithography to fabricate nanophotonic waveguides. Using both end-fire measurements and grating-based fibre couplers, we measured propagation losses as low as 0.24 dB/mm for photonic wires. We also demonstrated functional photonic wire components, like racetrack resonators, with a $Q = 12,000$. For photonic crystals, propagation losses are 7.5 dB/mm.

Acknowledgements

This work was supported by the EU through the IST-PICCO project. Part of this work was carried out for the Belgian IAP PHOTON network.

W. Bogaerts, P. Dumon, and B. Luyssaert thank the Flemish Institute for the Industrial Advancement of Scientific and Technological Research (IWT) for a specialization grant. J. Van Campenhout was supported by the Flemish Fund for Scientific Research (FWO-Vlaanderen) through a doctoral fellowship. D. Van Thourhout is supported through a return grant of the Belgian Federal Science Policy Office.

The authors would also like to thank D. Vangoidenhoven for the wafer exposures, R. de Ruyter and J. Mees for their work on the mask design, and J. Wouters for the extensive work on the etch development. Also many thanks to the people of the P-Line for the processing.

References

- [1] J.D. Joannopolous, R. Meade, J. Winn, *Photonic Crystals—Molding the Flow of Light*, Princeton University Press, Princeton, NJ, 1995.
- [2] W. Bogaerts, V. Wiaux, D. Taillaert, S. Beckx, B. Luyssaert, P. Bienstman, R. Baets, Fabrication of photonic crystals in Silicon-on-insulator using 248-nm deep UV lithography, *IEEE J. Sel. Topics. Quant. Electron.* 8 (4) (2002) 928–934.
- [3] W. Bogaerts, R. Baets, P. Dumon, V. Wiaux, S. Beckx, D. Taillaert, B. Luyssaert, J. Van Campenhout, P. Bienstman, D. Van Thourhout, Nanophotonic waveguides in Silicon-on-insulator fabricated with CMOS technology, *J. Lightwave Technol.* (2004) in press.
- [4] W. Bogaerts, D. Taillaert, B. Luyssaert, P. Dumon, J. Van Campenhout, P. Bienstman, D. Van Thourhout, R. Baets, V. Wiaux, S. Beckx, Basic structures for photonic integrated circuits in Silicon-on-insulator, *Opt. Expr.* 12 (8) (2004) 1583–1591.
- [5] D. Taillaert, W. Bogaerts, P. Bienstman, T. Krauss, P. Van Daele, I. Moerman, S. Verstuyft, K. De Mesel, R. Baets, An out-of-plane grating coupler for efficient butt-coupling between compact planar waveguides and single-mode fibers, *IEEE J. Quant. Electron.* 38 (7) (2002) 949–955.
- [6] J. Vaughan, *The Fabry–Perot interferometer*, Adam Hilger, Bristol, 1989.
- [7] P. Dumon, W. Bogaerts, V. Wiaux, J. Wouters, S. Beckx, J. Van Campenhout, D. Taillaert, B. Luyssaert, P. Bienstman, D. Van Thourhout, R. Baets, Low-loss SOI photonic wires and ring resonators fabricated with deep UV lithography, *IEEE Photon Technol. Lett.* 16 (5) (2004) 1328–1330.